École Polytechnique de Louvain

LINMA2361- Nonlinear dynamical systems Analysis of the Collisionless Singular Cucker-Smale Model with Decentralized Formation Control

Author:
Antoine Springael - 61372000

Professors:
Pierre-Antoine Absil
Estelle Massart

January 12, 2025

Contents

1 Introduction

This work is based on the article *"A Collisionless Singular Cucker-Smale Model with Decentralized Formation Control"* by Young-Pil Choi, Dante Kalise, Jan Peszek, and Andrés A. Peters [1]. The article investigates a multi-agent system (MAS) inspired by Cucker-Smale dynamics, with a focus on achieving collision avoidance and decentralized formation control. It proposes a singular interaction kernel and feedback control laws designed to induce specific spatial patterns while avoiding collisions. The article is available on arXiv at `https://arxiv.org/abs/1807.05177`.

The main objective of this project is to build upon the findings of the original article by exploring the behavior of the model under various modifications and analyzing how these changes influence the system's performance. This report aims to summarize the mathematical framework and key results of the original article, investigate the impact of different network configurations on the dynamics, and explore alternative approaches to the communication and control mechanisms. Additionally, this work includes a parametric study to evaluate the sensitivity of the system and provides new visualizations and numerical experiments to extend the analysis presented in the original study.

This report is structured as follows. The next section reviews the mathematical foundations of the collisionless singular Cucker-Smale model, including its interaction kernel and decentralized control laws. Then, a comparative analysis of network topologies and communication functions is performed, accompanied by numerical simulations illustrating their effects. Following that, a parametric study is conducted to investigate the influence of key factors on the system's behavior. Finally, the results are discussed in the context of the original findings, and potential improvements and directions for future research are proposed.

The implementation is performed using Python, leveraging libraries such as NumPy for numerical computations and Matplotlib for visualization. All the code is fully available here : `https://github.com/Antoine-EPL/Project_LINMA2361`.

2 Theoretical foundations

In this section, we briefly present the theoretical framework of the collisionless singular Cucker-Smale model with decentralized formation control, as introduced in [1]. As the theory is comprehensively detailed in the original article, we focus on the principal results that underpin the system's dynamics, collision avoidance, and pattern formation.

2.1 System description

The system models the dynamics of a group of n agents in $\mathbb{R}^d$ through their positions $x_i(t) \in \mathbb{R}^d$ and velocities $v_i(t) \in \mathbb{R}^d$, $i = 1, \dots, n$, which evolve for $t > 0$ according to the following system of equations:

$$\begin{aligned} \frac{dx_i(t)}{dt} &= v_i(t), \\ \frac{dv_i(t)}{dt} &= \frac{K}{n} \sum_{j=1}^{n} \psi(r_{ij}(t))(v_j(t) - v_i(t)) + Mu_i(t), \end{aligned} \tag{1}$$

with initial conditions:

$$x_i(0) = x_i^0, \quad v_i(0) = v_i^0, \quad i = 1, \dots, n. \tag{2}$$

Here, $r_{ij}(t) = \|x_j(t) - x_i(t)\|$ denotes the Euclidean distance between agents i and j at time t. The meaning of the first equation is clear. The second equation quantifies the acceleration of each agent, incorporating two key components: a velocity alignment term and an external control term.

The first term, the velocity alignment term, models the tendency of agents to align their velocities with those of their neighbors. The parameter $K \geq 0$ controls the strength of this alignment. The function

$\psi : \mathbb{R}_+ \to \mathbb{R}_+$ is the interaction kernel, which determines how strongly agents influence one another based on their relative distances. Typically, ψ is assumed to be non-increasing and nonnegative, meaning that closer agents exert a stronger influence. In this work, the model adopts a singular kernel:

$$\psi(r) = \frac{1}{r^\alpha}, \quad \alpha > 0, \tag{3}$$

which diverges when the distance between two agents r tends towards 0. This choice ensures a strong repulsive effect when agents are very close, effectively preventing collisions without requiring an additional explicit repulsive term. While other forms of ψ exist, the singular kernel is particularly advantageous in this context as it simplifies the dynamics while preserving collision-avoidance properties [2].

The second term, the external control term, is designed to enforce a desired spatial configuration among the agents. The parameter $M \geq 0$ modulates the strength of this control. Unlike centralized control approaches, which require global knowledge of the system, this control law is decentralized and depends only on local information about neighboring agents. Specifically, it is defined as follows:

$$\begin{aligned} u_1(t) &= -\phi(\|x_1(t) - x_2(t) - z_1\|^2)(x_1(t) - x_2(t) - z_1), \\ u_n(t) &= \phi(\|x_{n-1}(t) - x_n(t) - z_{n-1}\|^2)(x_{n-1}(t) - x_n(t) - z_{n-1}), \\ u_i(t) &= \phi(\|x_{i-1}(t) - x_i(t) - z_{i-1}\|^2)(x_{i-1}(t) - x_i(t) - z_{i-1}) \\ &\quad - \phi(\|x_i(t) - x_{i+1}(t) - z_i\|^2)(x_i(t) - x_{i+1}(t) - z_i), \end{aligned} \tag{4}$$

for $i = 2, \ldots, n-1$, where $z_i \in \mathbb{R}^d$, $i = 1, \ldots, n-1$ encodes the desired relative positioning between agents and $\phi(r)$ is a regular communication weight, determining the influence of deviations from the desired relative positions, of the form:

$$\phi(r) = \frac{1}{(1+r)^\beta}, \quad \beta > 0. \tag{5}$$

2.2 Key theoretical results

The system exhibits three fundamental behaviors: collision avoidance, flocking, and pattern formation. These results are analyzed through energy estimates that describe the system's evolution over time. The total energy of the system consists of a kinetic component and a potential component, defined as follows:

$$E(x,v) = E_1(v) + E_2(x), \quad E_1(v) = \frac{1}{2}\|v\|^2, \quad E_2(x) = \frac{M}{2}\sum_{i=2}^{n}\int_0^{\|x_{i-1}-x_i-z_{i-1}\|^2} \phi(r)\, dr. \tag{6}$$

The term $E_1(v)$ corresponds to the kinetic energy, representing the velocity alignment among agents, while $E_2(x)$ corresponds to the potential energy induced by the decentralized control law. The dissipation rate of the system, linked to the interaction kernel ψ, is given by:

$$D(x,v) = \frac{K}{2n}\sum_{i,j=1}^{n} \psi(r_{ij})\|v_i - v_j\|^2. \tag{7}$$

2.2.1 Energy conservation and dissipation

The evolution of the system is governed by the following relationship:

$$\frac{d}{dt}E_1(v(t)) + \frac{d}{dt}E_2(x(t)) + D(x(t), v(t)) = 0, \quad \forall t \geq 0, \tag{8}$$

which shows that the total energy of the system is non-increasing over time. Additionally, the system preserves two key invariants. The average velocity and average position of all agents, defined as:

$$\bar{v} = \frac{1}{n}\sum_{i=1}^{n} v_i, \quad \bar{x} = \frac{1}{n}\sum_{i=1}^{n} x_i, \tag{9}$$

remain constant in time. Without loss of generality, these averages are often assumed to be zero for simplicity, i.e., $\bar{v} = 0$ and $\bar{x} = 0$.

2.2.2 Collision avoidance

The singular kernel $\psi(r)$ defined in (3) with $\alpha \geq 1$ ensures collision avoidance under suitable initial conditions. Specifically, if the initial distances between agents satisfy $r_{ij}(0) > 0$ for all $1 \leq i \neq j \leq n$, then the system (1) admits a unique global smooth solution satisfying:

$$\min_{1 \leq i \neq j \leq n} r_{ij}(t) > 0, \quad \forall t \geq 0. \tag{10}$$

Note that it was shown in [2] that under certain conditions, it is possible to modify the singular kernel in order to impose a minimal distance δ between the agents for any time $t \geq 0$.

2.2.3 Flocking behavior

The system (1) achieves flocking, meaning that agent velocities converge to a common value while relative positions remain uniformly bounded. Specifically, if the total energy, as defined in (6), is finite at $t = 0$, the conditions required for collision avoidance are satisfied, and $\beta \leq 1$, then the following holds:

$$\sup_{t \geq 0} \max_{1 \leq i \neq j \leq n} r_{ij}(t) < \infty \quad \text{and} \quad \lim_{t \to \infty} \max_{1 \leq i \neq j \leq n} \|v_i(t) - v_j(t)\| = 0. \tag{11}$$

This result indicates that agents remain in a cohesive group and align their velocities asymptotically to a common value. It is worth noting that a similar result can be obtained for the case $\beta > 1$, provided additional conditions on the initial quantities are satisfied, as detailed in the original article.

2.2.4 Pattern formation

The decentralized control law ensures that agents converge to a desired spatial configuration as $t \to \infty$, provided that collisions are avoided asymptotically. Formally, if the conditions for collision avoidance and flocking behavior are met, the following holds:

$$\lim_{t \to \infty} \big(x_i(t) - x_{i+1}(t)\big) = z_i, \quad \forall i = 1, \ldots, n-1. \tag{12}$$

This result guarantees that the relative positions between consecutive agents asymptotically approach the desired configuration encoded by z_i.

2.3 Simulation of the model

This section aims to reproduce numerically the behavior of the flocking system as described in the original article, in order to gain a better understanding of its dynamics. Therefore, we consider a basic case to illustrate the core properties of the model. Note that degenerate cases are presented in the article but here we focus on non-degenerate cases.

Specifically, we simulate a circular formation pattern in a two-dimensional space with $n = 10$ agents. The parameters are chosen as $K = 10$, $M = 50$, $\alpha = 1.1$, and $\beta = 0.5$. These values match those of the first example in the article and will be revisited later in this report for further analysis. The initial positions and velocities of the agents are selected randomly, but with an imposed zero average. This choice simplifies the visualization of the results, as the agents converge to a centered formation with null velocities (due to the fact that these quantities are invariants of the system). However, if a nonzero initial average velocity were imposed, the agents would converge to a moving formation, mimicking, for example, a flock of birds in motion. In the snapshots, agents are represented as blue circles, which should be interpreted as points, and their velocities are shown as arrows. The arrows are normalized to have a constant length for better visualization, although the velocities tend to zero in this case due to the imposed zero average initial velocity.

Note that an animation of the movement of the agents and the real-time updating of the various metrics is available on the accompanying GitHub repository.

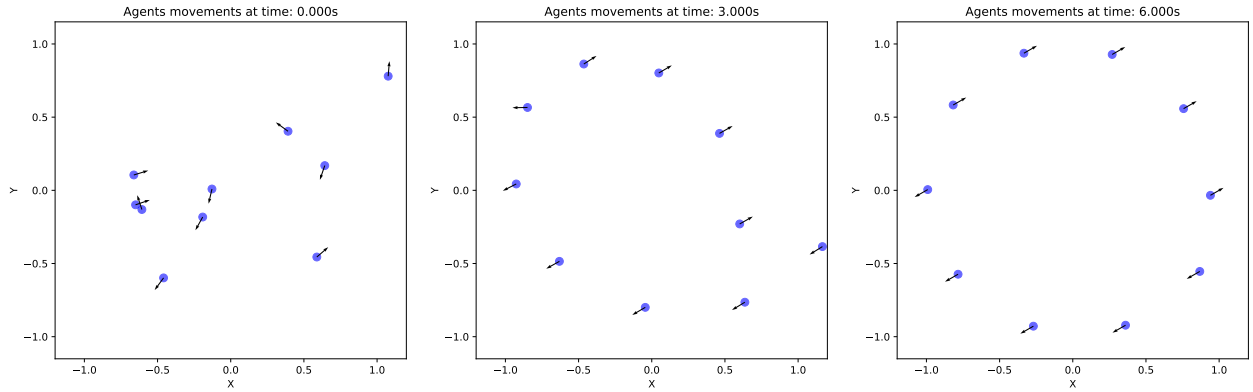

Figure 1: Snapshots of the circular formation simulation at different times.

When analyzing the snapshots in Figure 1, we observe how the agents evolve towards the desired circular formation. Initially, the agents are randomly distributed. By the intermediate snapshot at 3 seconds, the agents are seen "unfolding" into a circular pattern, adjusting their positions relative to their neighbors. This behavior is driven by the decentralized control term, which ensures that each agent maintains the desired relative positioning with its neighbors. The first and last agents, being connected to only one neighbor each, exhibit more pronounced adjustments. By 6 seconds, the agents have achieved the final circular formation. This raises an interesting question: could alternative dependency networks lead to a more fluid formation process? This question is explored further in the next section. To gain further insights into the dynamics, we analyze three key metrics over time: total energy, minimum distance between agents, and maximal velocity difference, as shown in Figure 2.

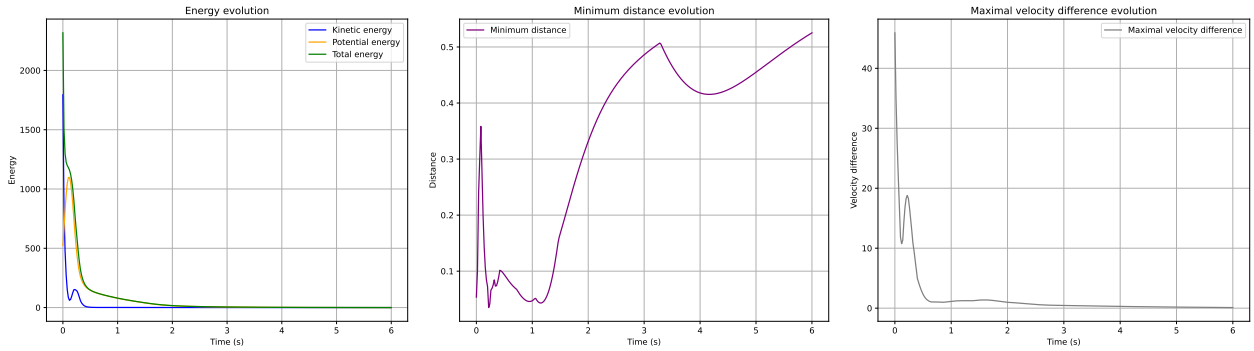

Figure 2: Evolution of key metrics during the simulation.

The metrics in Figure 2 confirm several theoretical predictions. The total energy is monotonically decreasing, as expected from the energy dissipation relationship. Observing the plot of the maximal velocity difference, we note a peak around 0.25 seconds. This phenomenon occurs because two agents initially positioned close together in the first snapshot of Figure 1 repel each other strongly due to the singular interaction kernel. This behavior is also reflected in the minimum distance plot, where the distance between these two agents (who were the closest) increases sharply at the same time. Despite this peak, the minimal distance between agents remains strictly positive throughout the simulation, confirming the absence of collisions.

In the early stages of the simulation, we observe significant variations in the minimal distance due to the initial random distribution of agents. However, as the formation progresses, these variations become smoother, reflecting the stabilization of the system. For the maximal velocity difference, aside from the aforementioned peak at 0.25 seconds, it converges to zero, consistent with the flocking estimates.

Overall, the agents successfully avoid collisions and achieve the desired circular formation, aligning with the theoretical results.

3 Network structures and their influence

The results of our earlier simulations underscore the importance of network topology in influencing collective dynamics. Specifically, the observations indicate that sparse connections may hinder pattern formation, leading to slower or incomplete convergence to the desired configuration. Motivated by these findings and inspired by [3], this section generalizes the Cucker-Smale model by introducing alternative network structures. While [3] incorporates stochastic dynamics, we focus exclusively on deterministic systems to analyze how different network topologies affect flocking behavior and formation control.

3.1 Generalized network dynamics

The original model assumes that each agent interacts with only its two immediate neighbors (one for the first and last agents), which results in a linear chain structure for the control graph. This configuration, while effective in simple cases, may not be optimal for more complex patterns or realistic scenarios. By generalizing the graph structures used for agent interactions, we aim to improve the system's performance and make it potentially more realistic.

3.1.1 Graph representation and dynamics

The generalized model associates distinct graph structures with velocity alignment and formation control. Let $G_\psi = (V, E_\psi)$ denote the graph associated with velocity alignment, and $G_\phi = (V, E_\phi)$ the graph associated with decentralized formation control. The vertex set $V = \{1, \dots, n\}$ represents the agents, while the edge sets $E_\psi, E_\phi \subseteq V \times V$ encode the connections specific to each interaction type. In this study, we assume symmetric graphs (ensuring mutual influence) and connected graphs (ensuring that there is a path between any two agents). We exclude also self-loop in the graph. However, hierarchical or asymmetric interactions can also be modeled by relaxing the symmetry condition. The neighborhood of an agent i in graph G_ψ is defined as:

$$\mathcal{N}_i^\psi = \{j \in V \mid (j, i) \in E_\psi\},$$

with a similar definition for $\mathcal{N}_i^\phi$. Using this generalized framework, the dynamics of each agent are described by:

$$\begin{aligned} \frac{dx_i(t)}{dt} &= v_i(t), \\ \frac{dv_i(t)}{dt} &= \sum_{j \in \mathcal{N}_i^\psi} \psi(r_{ij}(t))(v_j(t) - v_i(t)) + M u_i(t), \end{aligned}$$

where the decentralized control term $u_i(t)$ is given by:

$$u_i(t) = \sum_{j \in \mathcal{N}_i^\phi} \phi(\|x_j(t) - x_i(t) - (z_j - z_i)\|^2)(x_j(t) - x_i(t) - (z_j - z_i)).$$

Here, $z_i - z_j$ specifies a desired relative positioning between agents x_i and x_j, encoded by the predefined spatial configuration z. This generalization allows the control term to enforce decentralized formation in heterogeneous networks.

3.1.2 Energy in the generalized framework

The system's dynamics are analyzed through energy estimates, modified to incorporate the effects of network structures. The total energy of the system combines kinetic energy, potential energy, and dissipation. Note that there is no longer any mention of the fact that the total energy of the system is non-increasing over time. The kinetic energy remains unchanged and is expressed as:

$$E_1(v) = \frac{1}{2} \sum_{i=1}^{n} \|v_i\|^2.$$

The potential energy, reflecting the connectivity of G_ϕ, is given by:

$$E_2(x) = \frac{M}{2} \sum_{(i,j)\in E_\phi} \int_0^{\|x_j - x_i - (z_j - z_i)\|^2} \phi(r)\, dr.$$

The dissipation term accounts for velocity alignment over G_ψ:

$$D(x, v) = \frac{K}{2} \sum_{(i,j)\in E_\psi} \psi(r_{ij}) \|v_i - v_j\|^2.$$

3.2 Types of graph structures

Different types of network topologies will lead to different evolutions in agent movement and different convergence behaviours. To illustrate this, we consider the four following graph types inspired by [3]:

- G_0: A fully connected graph where every agent interacts with all others.
- G_1: A graph with only three central vertices connected to all others, while the remaining vertices are connected only to their neighbors.
- G_2: A path graph where each agent (except the starting and terminal vertices) interacts only with its immediate neighbors, forming a linear chain.
- G_3: A graph where every vertex is connected to its neighbors and, additionally, vertices $i \equiv 1 \pmod{10}$ are connected to all other vertices.

Note that, in comparison with the article, our graph G_3 corresponds to their graph G_4. These graph types are illustrated in Figure 3. The graph G_0, used for velocity alignment in the base model, ensures global communication, whereas G_2, employed for the control law, represents localized interactions. Intuitively, denser graphs improve alignment but increase computational complexity. Balancing graph density and computational efficiency is a key consideration for designing effective multi-agent systems.

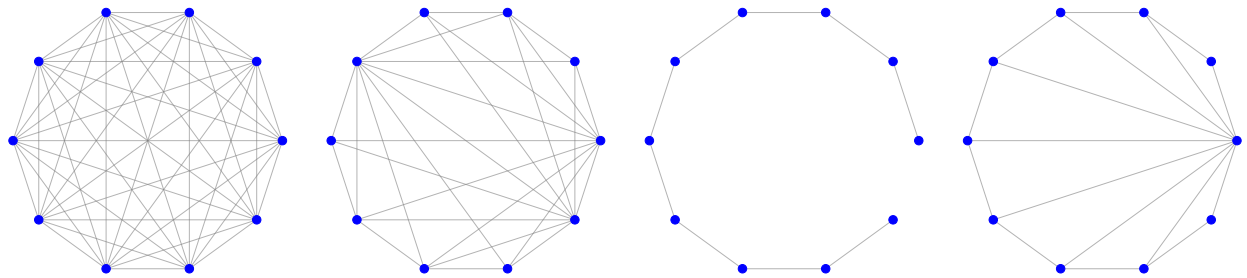

(a) G_0 ($|E| = 45$) (b) G_1 ($|E| = 29$) (c) G_2 ($|E| = 9$) (d) G_3 ($|E| = 17$)

Figure 3: Illustration of different graph types for $n = 10$ agents.

3.3 Impact of network topology on total energy

To evaluate the impact of network topology, we perform simulations using the same parameters as in the initial circular pattern ($K = 10$, $M = 50$, $\alpha = 1.1$, $\beta = 0.5$). The objective is to identify the combination of graphs G_ψ and G_ϕ that balance sparsity while maintaining a smooth convergence. The aim of graph sparsity is directly linked to computational complexity.

Energy serves as a key indicator in this study, as it tends toward zero as the formation process completes. Faster and smoother energy decay suggests a more efficient formation. While alternative metrics, such as energy dissipation rates, could be relevant for specific applications, our analysis emphasizes energy minimization as a measure of efficiency.

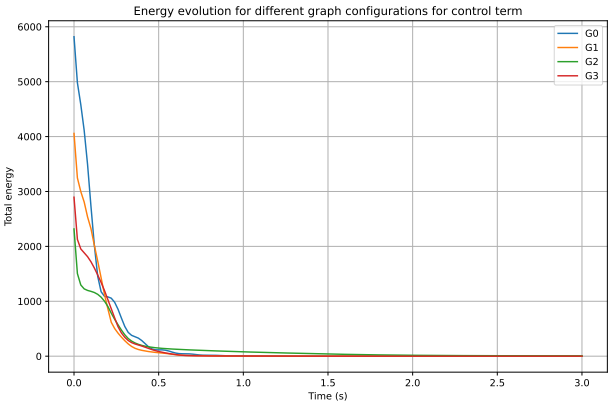

(a) Graph G_ψ: G_0

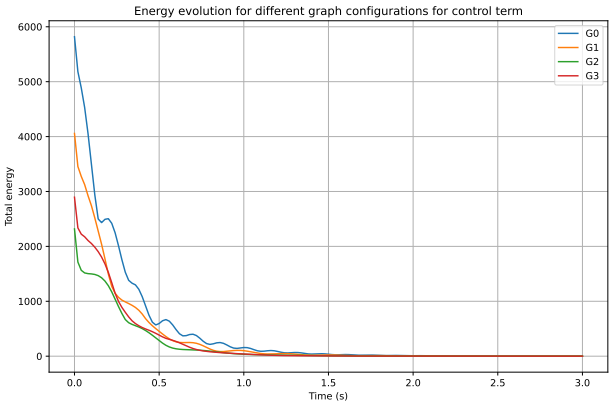

(b) Graph G_ψ: G_1

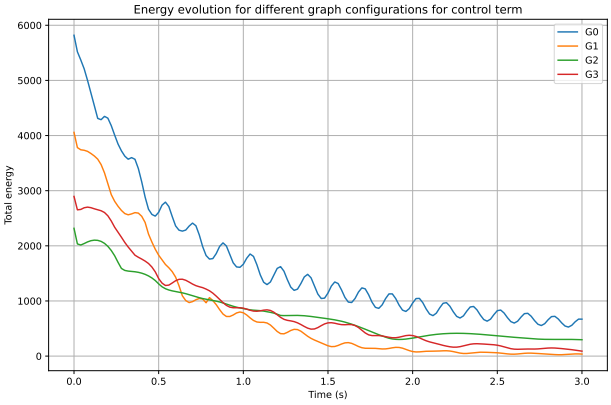

(c) Graph G_ψ: G_2

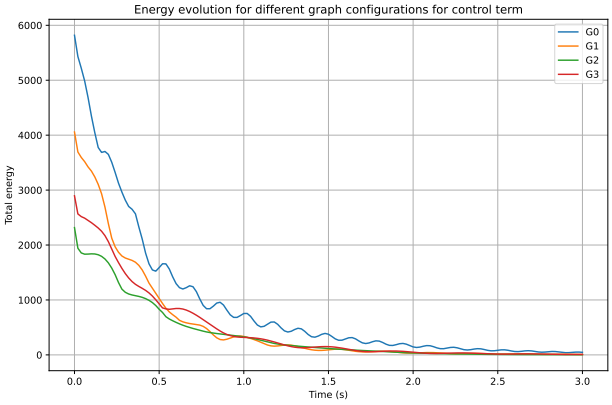

(d) Graph G_ψ: G_3

Figure 4: Energy evolution for various G_ϕ configurations with fixed G_ψ.

From Figure 4, we observe that dense graphs for G_ψ, such as G_0 or G_1, lead to faster energy dissipation compared to sparse (G_2) or hybrid (G_3) configurations. However, hybrid configurations sometimes offer a good trade-off between computational complexity and convergence speed.

When G_ψ is fixed as G_0 (complete graph), we observe that all graph types for G_ϕ outperform the base case $G_\phi = G_2$. This result highlights the inefficiency of sparse control graphs in fully connected velocity alignment networks. However, for other G_ψ configurations, such as $G_\psi = G_2$ or G_3, the graph ($G_\phi = G_2$) demonstrates competitive performance compared to denser configurations.

A notable observation is that combinations with $G_\phi = G_0$ almost always exhibit the worst performance. This is likely due to the high connectivity of G_ϕ, where the movement of a single agent induces oscillatory effects throughout the network, leading to fluctuations in the total energy. These oscillations reduce the smoothness of the convergence process and can delay the overall formation stabilization.

For applications where computational cost is not a concern, dense configurations such as $G_\psi = G_0$ and $G_\phi = G_1$ provide the fastest convergence. However, if a balance between computational complexity and convergence speed is desired, hybrid combinations, such as $G_\phi = G_2$ or G_3 with $G_\psi = G_1$ or G_3, are recommended. These configurations achieve reasonable performance while reducing the number of connections required for communication and control.

The simulation results are illustrated through animations available on the accompanying GitHub repository. These animations show the temporal evolution of the agents for two specific combinations: $G_\psi = G_0$ with $G_\phi = G_1$, and $G_\psi = G_1$ with $G_\phi = G_3$. In both cases, the agents converge toward the desired circular formation significantly faster than in the base case where $G_\psi = G_2$ and $G_\phi = G_2$.

4 Impact of parameters

Throughout this report, we have consistently used the parameter values provided in the original article without optimizing them. It is now time to explore the impact of these parameters on the system's behavior. Specifically, we will use the same baseline scenario for consistency, ensuring a fair comparison. For this analysis, we consider the graph configurations $G_\psi = G_1$ and $G_\phi = G_3$, as they provide a good balance between rapid convergence and computational complexity. However, since they are not the optimal configuration, the goal here is to study the effects of varying the four key parameters: α, β, K, and M. It is worth noting that, as previously discussed, α must satisfy $\alpha \geq 1$ to ensure collision avoidance, while we will focus on $\beta \leq 1$, which aligns with the typical cases considered in the literature.

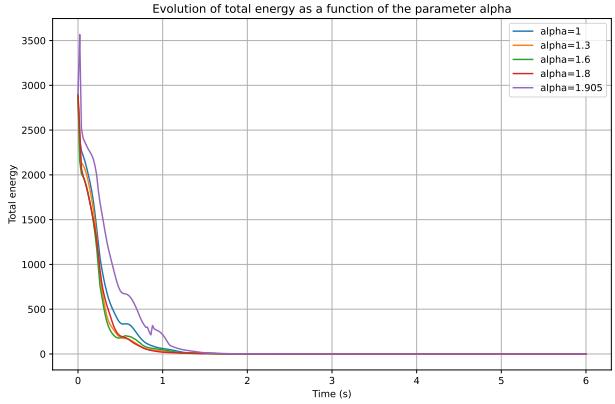

(a) Effect of α

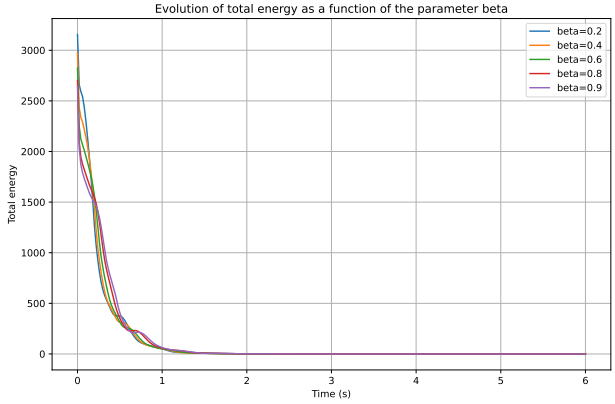

(b) Effect of β

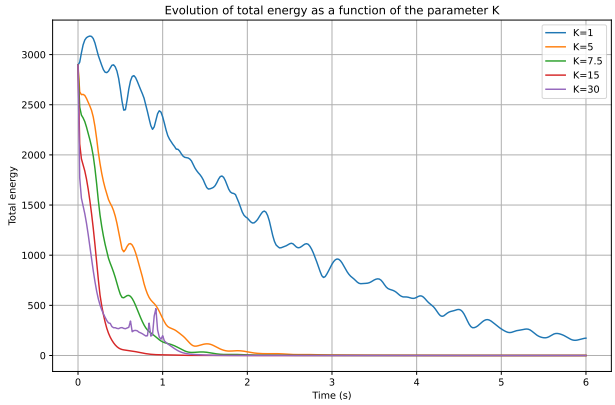

(c) Effect of K

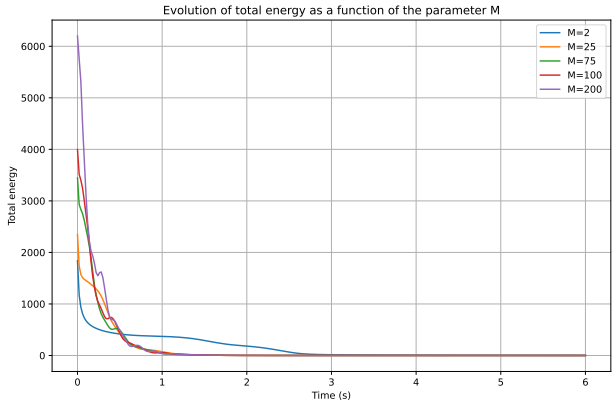

(d) Effect of M

Figure 5: Analysis of the impact of α, β, K, and M on energy evolution.

The parameter α directly influences the interaction kernel $\psi(r)$, which governs velocity alignment. Our analysis reveals minimal impact of α on energy dissipation rates for values near the baseline. However, increasing α beyond 1.9 leads to significant energy fluctuations. For instance, with $\alpha = 1.905$, the energy fluctuations become increasingly pronounced, which could destabilize the system.

The parameter β appears in the communication weight $\phi(r)$, which influences potential energy. Variations in β have minimal impact on the energy dissipation rate. The most noticeable effect is on the initial energy levels: smaller values of β result in higher initial potential energy.

The parameter K, which modulates the strength of velocity alignment, exhibits distinct effects on the system's behavior. For small values of K, such as $K = 1$, the energy dissipation is slow, and fluctuations are evident throughout the process. At the other extreme, when K reaches 30, we observe abrupt and destabilizing fluctuations in energy. Optimal performance occurs at intermediate values of K. For instance, $K = 15$ achieves faster convergence than $K = 7.5$ or $K = 5$, with fewer oscillations.

The parameter M, which scales the decentralized control input, has a pronounced impact on convergence rates. For small values, such as $M = 1$, the convergence is extremely slow, as the control input is insufficient to drive agents toward the desired configuration. In these cases, potential energy remains high for extended periods, reflecting the system's delayed response. Increasing M accelerates the initial rate of convergence but plateaus quickly. For example, $M = 25$ achieves similar convergence rates to $M = 200$, despite the latter resulting in significantly higher initial potential energy. This suggests that beyond a certain threshold, further increases in M do not meaningfully enhance performance but instead amplify energy costs.

Animations illustrating the agent dynamics for various parameter configurations are available on the GitHub repository. These visualizations confirm the trends observed in energy dissipation. For instance, with $G_\psi = G_1$, $G_\phi = G_3$, and optimized parameters, the agents converge rapidly to the desired circular formation, far outperforming the baseline configuration

5 Demonstration of advanced formations

While the circular formation has been used as a baseline throughout this study, the flexibility of the model enables the generation of more complex spatial patterns. In this section, we demonstrate two specific formations: a π-shaped curve and an ω-shaped curve. These formations were achieved using the parameters $\alpha = 1.0$, $\beta = 0.5$, $K = 450$, and $M = 150$. The graph configurations were set to $G_\psi = G_0$ and $G_\phi = G_1$. The parameter choices align with the findings of the parameter study conducted earlier in this report, with the exception of K, which was significantly increased to ensure the formation could be achieved within a reasonable timeframe. This adjustment was likely necessary due to the larger number of agents and their distribution over a wider area, requiring stronger velocity alignment to maintain cohesion. Note, however, that these parameters were not optimized for efficiency but were selected to achieve the desired configurations within a manageable timeframe. The specific curves used for the formations were generated with Wolfram Alpha, allowing precise definitions of complex shapes.

Figure 6 shows the evolution of the agents as they converge to the desired π-shaped formation.

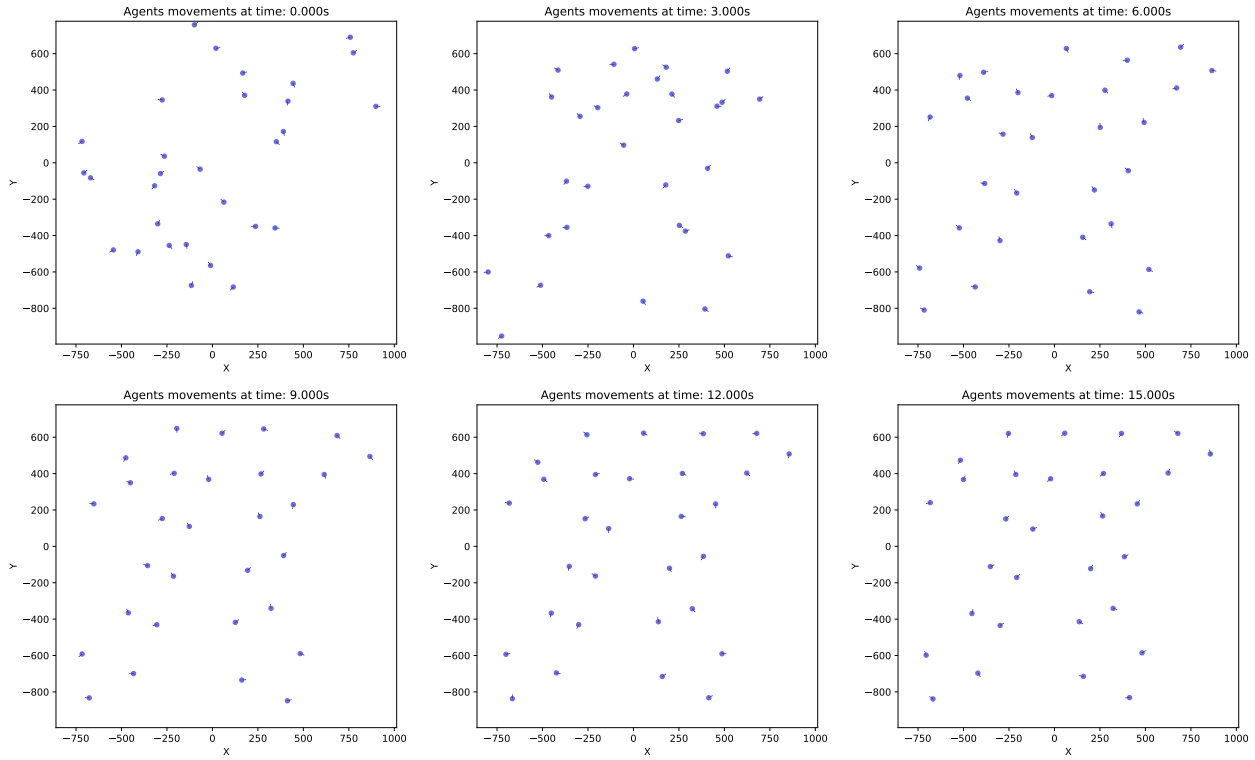

Figure 6: Snapshots of the π-shaped formation simulation at different times.

The desired formation begins to emerge around $t = 6$ seconds. Between $t = 9$ and $t = 15$ seconds, the agents exhibit oscillatory behavior as they adjust to achieve perfect alignment with the target configuration. While these oscillations are not visible in the static snapshots, they are clearly observed in the animations available on the GitHub repository. The snapshots, however, do capture the progressive adjustments made by the agents to reach their final positions.

The ω-shaped formation was achieved using the same parameter settings and graph configurations as the π-shaped formation. Figure 7 illustrates the evolution of the agents toward this complex pattern.

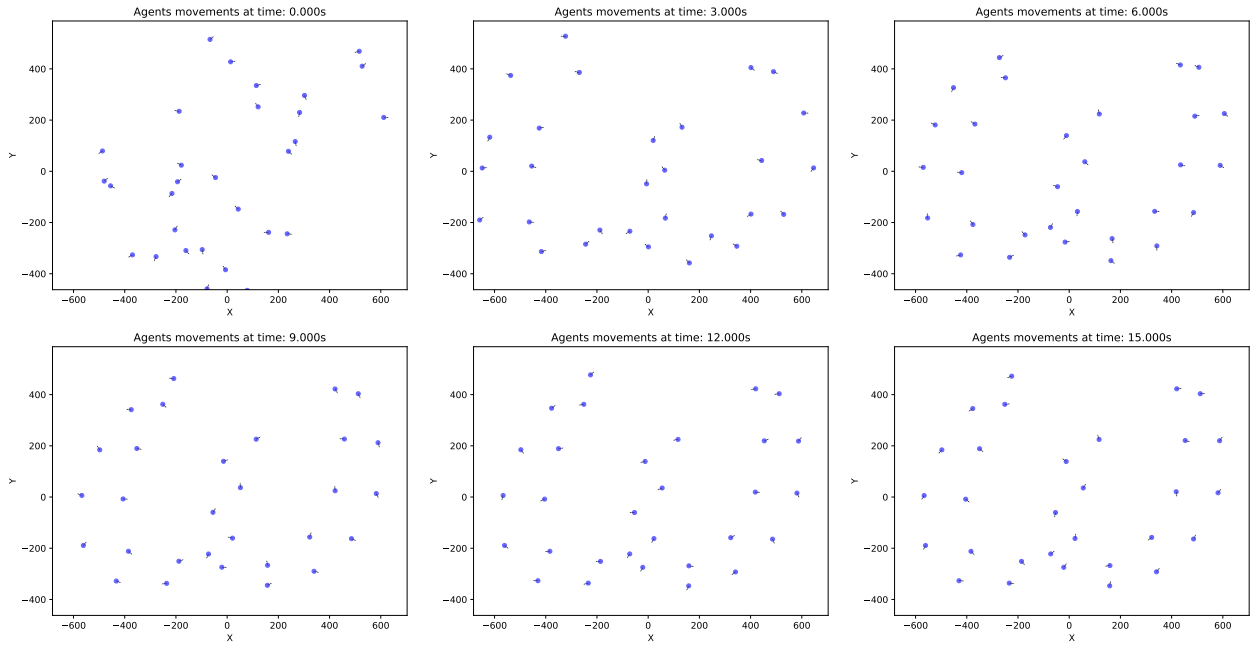

Figure 7: Snapshots of the ω-shaped formation simulation at different times.

As with the π-shaped formation, the target shape becomes recognizable around $t = 6$ seconds. Oscillatory adjustments persist until the agents stabilize, reaching the final configuration by $t = 15$ seconds. These oscillations are similarly visible in the animations, while the snapshots capture the agents' progressive refinement of their positions.

6 Conclusion

This report has explored the behavior and flexibility of the generalized Cucker-Smale model through the lens of a simple yet illustrative example. Starting with a baseline circular formation, we analyzed the impact of different network configurations and graph structures on the system's dynamics. By varying the connectivity patterns for velocity alignment and decentralized control, we highlighted how the choice of network topology influences energy dissipation, convergence speed, and computational complexity.

In addition to network structures, a detailed parameter study provided insights into the roles of key model parameters, such as α, β, K, and M. This analysis revealed how these parameters interact with the network configuration to drive the system toward its desired formation. While the focus remained on relatively straightforward scenarios, the findings demonstrated the model's robustness and adaptability in achieving complex spatial patterns, as evidenced by the π- and ω-shaped formations.

Future work could focus on analyzing parameters in more complex scenarios and exploring alternative communication weights to uncover new behaviors. These extensions would further demonstrate the versatility and potential applications of this model in multi-agent systems.

References

[1] CHOI, Young-Pil, KALISE, Dante, PESZEK, Jan, et al. *A collisionless singular Cucker-Smale model with decentralized formation control*. SIAM Journal on Applied Dynamical Systems, 2019, vol. 18, no 4, p. 1954-1981.

[2] CARRILLO, José A., CHOI, Young-Pil, MUCHA, Piotr B., and al. *Sharp conditions to avoid collisions in singular Cucker–Smale interactions*. Nonlinear Analysis: Real World Applications, 2017, vol. 37, p. 317-328.

[3] CHOI, Young-Pil, OH, Doeun, and TSE, Oliver. *Controlled pattern formation of stochastic Cucker–Smale systems with network structures*. Communications in Nonlinear Science and Numerical Simulation, 2022, vol. 111, p. 106474.